nature photonics

ARTICLES

PUBLISHED ONLINE: 10 AUGUST 2015 | DOI: 10.1038/NPHOTON.2015.150

Inverse four-wave mixing and self-parametric amplification in optical fibre

Sergei K. Turitsyn[1,2]*, Anastasia E. Bednyakova[2,3], Mikhail P. Fedoruk[2,3], Serguei B. Papernyi[4] and Wallace R. L. Clements[4]

An important group of nonlinear processes in optical fibre involve the mixing of four waves due to the intensity dependence of the refractive index. It is customary to distinguish between nonlinear effects that require external/pumping waves (cross-phase modulation and parametric processes such as four-wave mixing) and those arising from self-action of the propagating optical field (self-phase modulation and modulation instability). Here, we present a new nonlinear self-action effect—self-parametric amplification—which manifests itself as optical spectrum narrowing in normal dispersion fibre, leading to very stable propagation with a distinctive spectral distribution. The narrowing results from inverse four-wave mixing, resembling an effective parametric amplification of the central part of the spectrum by energy transfer from the spectral tails. Self-parametric amplification and the observed stable nonlinear spectral propagation with a random temporal waveform can find applications in optical communications and high-power fibre lasers with nonlinear intracavity dynamics.

Nonlinear fibre optics is a research field at the two-way interface of fundamental nonlinear physics and fibre-optic engineering that encompasses diverse areas of science and technology. Nonlinear effects in optical fibre are critically important for various practical applications ranging from telecommunications to medical fibre lasers (see, for example, refs 1–6 and references therein). However, nonlinear fibre optics is also a remarkable and versatile testbed for the experimental probing of the ideas and concepts of fundamental nonlinear science[5,7–13]. This, in turn, means that fibre optics is an ideal platform for the invention and development of novel devices based on nonlinear design concepts with functionality not available in linear science engineering. Due to the relatively low threshold for the occurrence of nonlinear effects in fibre, they may adversely impact signal propagation in optical communications or indeed may be positively exploited for the development of all-optical devices for optical networks, fibre lasers, signal-processing components and many other applications.

Typically, fibre nonlinear effects are subdivided into two main categories: phenomena induced by the nonlinearities that arise from scattering (stimulated Brillouin scattering (SBS) and stimulated Raman scattering (SRS)) and those induced by the nonlinear effects due to the Kerr effect, that is, the intensity dependence of the refractive index (self-phase modulation (SPM), cross-phase modulation (XPM), four-wave mixing (FWM), modulation instability (MI) and parametric processes based on FWM[2,4]). The interaction of two or more waves with different frequencies may lead to power transfer between them according to the corresponding stimulated scattering or parametric processes. A subclass of such phenomena occurs in the degenerate case, when a single wave affects itself through the nonlinear response of the medium. This is called a self-action effect. Although differentiation among the various manifestations of the Kerr nonlinearity is somewhat artificial (as all elementary nonlinear processes resulting from the cubic nonlinearity can be treated formally as a mixing of four waves), from a practical viewpoint it is convenient to distinguish between nonlinear interactions of the optical field under consideration with external fields (for example, pumping waves) co-existing from the very outset (for instance, XPM and parametric processes) and self-action of the propagating light wave (for example, SPM and MI).

In general, optical nonlinear self-action effects may be both spatial (self-focusing, SPM and spatial MI) and temporal (SPM and

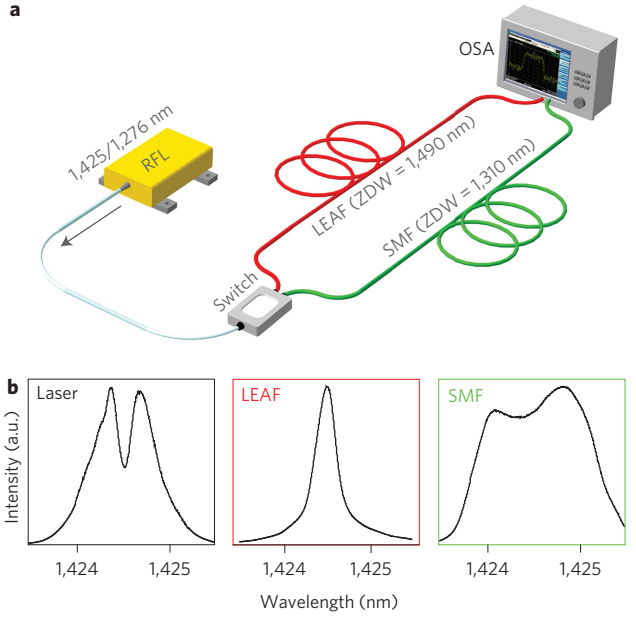

Figure 1 | Experimental observation of spectrum evolution in normal and anomalous dispersion fibres. a, Experimental set-up. **b**, Initial spectrum and spectrum after propagation in 100 km of LEAF and SMF-28 fibres. Power launched into each fibre = 1.5 W. OSA: optical spectrum analyser; RFL: Raman fibre laser.

[1]Aston Institute of Photonic Technologies, Aston University, Birmingham B4 7ET, UK. [2]Novosibirsk State University, Novosibirsk 630090, Russia. [3]Institute of Computational Technologies, SB RAS, Novosibirsk 630090, Russia. [4]MPB Communications Inc., Montreal, Quebec H9R 1E9, Canada. *e-mail: s.k.turitsyn@aston.ac.uk

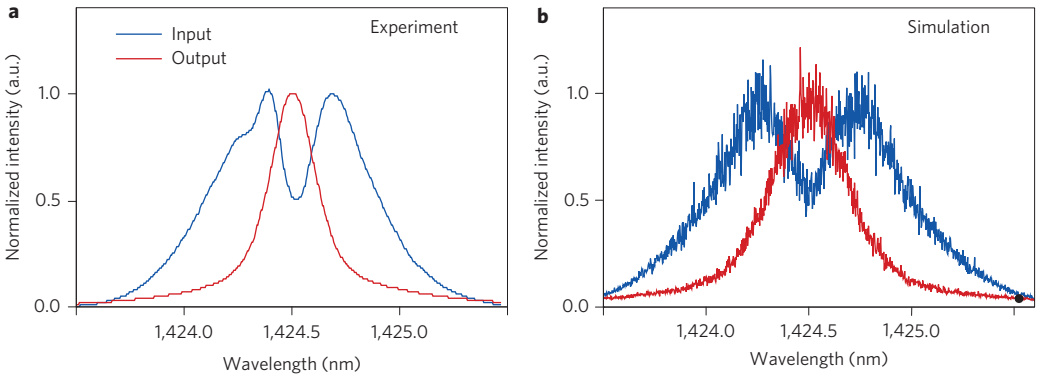

Figure 2 | Spectrum shape after signal propagation in LEAF fibre. a, Experiment and **b**, simulation. $P_0(0) = 1.5$ W, $L = 100$ km.

temporal MI). Self-action occurs when a propagating electromagnetic wave induces a refractive index change in the medium. The modified index of refraction in a fibre in turn affects the overall propagating field, producing effective self-action of the wave.

Optical parametric amplification (OPA) in fibres, pioneered by R. Stolen[14], is traditionally considered to be a process of energy transfer from pumping wave(s) to a signal wave. Recently, fibre OPA has become a booming area of research, with impressive demonstrations of the feasibility of low-noise parametric amplification in high-capacity optical communications[15–22]. These breakthroughs are greatly supported by recent progress in the development of efficient highly nonlinear fibres with a large ratio of the nonlinear coefficient to the attenuation parameter.

In this Article, we introduce a new nonlinear self-action effect in optical fibre, inverse FWM or self-parametric amplification (SPA), which occurs in normal dispersion optical fibres under certain conditions (as described in the following). Note that the term 'parametric amplification' is used here in a context that is different from the standard usage. Traditional parametric amplification is typically defined for monochromatic waves, but here we use this term for the relatively broad spectrum of a multi-longitudinal-mode Raman fibre laser. Moreover, the term 'amplification' here means only a redistribution of the energy due to inverse FWM and is applied only to the central part of the spectrum that is 'gaining' power at the expense of the energy decrease in the spectral tails of the field. However, we believe that this terminology helps to explain the underlying elementary processes and physics of the unusual nonlinear process demonstrated. We have observed experimentally and confirm through comprehensive numerical modelling that the spectral width of a signal produced by a Raman fibre laser (RFL) becomes narrower after propagation in a sufficient length of normal dispersion fibre. The resulting state, featuring a narrow spectrum and random temporal field distribution, propagates with remarkable stability, showing potential for applications in fibre lasers and optical communications. We present a basic theory of SPA that is confirmed by extensive numerical modelling and experimental observations.

Experimental set-up

We start with a description of the experiment that initiated this study, the experimental set-up of which is shown in Fig. 1a. In the first set of experiments an RFL[23] was operated at ~1,425 nm, and in the set of cross-check experiments presented at the end of this Article, an RFL operating at 1,276 nm was used. Both Raman lasers operated in the continuous-wave (c.w.) regime with a maximum output power of up to 2 W. The outputs were randomly polarized with a degree of polarization of <5%. It is widely known in fibre optics that nonlinear effects such as FWM and SPM typically manifest themselves as spectrum broadening when relatively high-power c.w. fields propagate in optical fibres[23–29]. A characteristic feature of the RFL, related to a high in-resonator power and the resulting in-cavity spectral broadening, is that its output spectrum has two peaks with a separation of 0.2–1 nm (Fig. 1b). The double-peaked structure of the output spectrum is the result of the FWM-induced spectral broadening inside the Raman converter cavity, which leads to a spectral breadth that exceeds the reflection bandwidth of the fibre Bragg grating (FBG) output coupler and therefore leads to radiation 'overflowing' the FBG reflector[23–30].

The laser radiation generated at 1,424.5 nm was launched into 100-km-long Corning LEAF (large effective area fibre) or single-mode fibre (SMF-28), with a zero-dispersion wavelength (ZDW) around 1,490 nm for LEAF and 1,310 nm for SMF-28. Light thus propagates in the region of normal dispersion for the LEAF fibre and in the region of anomalous dispersion for the SMF-28. The spectra at the input and output of the 100 km lengths of fibre were measured with an optical spectum analyser (OSA) with a resolution of 0.01 nm.

Narrowing of the optical spectra

The measured optical spectrum at the end of the LEAF fibre shows significant narrowing (Fig. 1b, LEAF), in sharp contrast to the typical nonlinear spectral broadening in SMF-28 (Fig. 1b, SMF) caused by FWM, which has been observed and studied in a number of experimental and theoretical publications[23,24,27–29,31,32]. Explaining this atypical narrowing effect is the aim of the present work.

Extensive numerical modelling of light generation in the RFL and its further propagation in the LEAF fibre fully confirms the observed unusual spectral behaviour of a nonlinear wave in a long fibre with normal dispersion. Signal evolution inside the laser cavity was modelled by the set of coupled modified nonlinear Schrödinger equations (NLSEs), taking into account dispersion, Kerr nonlinearity, Raman gain, depletion of the Raman pump wave and fibre losses. All details of the modelling are presented in refs 2 and 33 (see also Methods). Signal evolution in the LEAF fibre was computed using the standard NLSE[2].

The results of the experiments and numerical simulations presented in Figs 2 and 3 demonstrate spectral narrowing of the c.w. radiation with simultaneous temporal fluctuations. The initial spectrum was converted to a double-scale distribution (a bell-shaped peak in the centre but with exponentially decaying spectral tails introducing a second scaling parameter in the spectral distribution) at the LEAF output both in the experiment and simulation (Fig. 2). A stable spectrum evolution (after ~50 km) along the LEAF fibre is shown in Fig. 3a. We stress that the observed stabilization of the spectrum is a nontrivial nonlinear process. Intensive numerical modelling shows that this happens both in a fibre span with loss and in the corresponding lossless system. The spatiotemporal

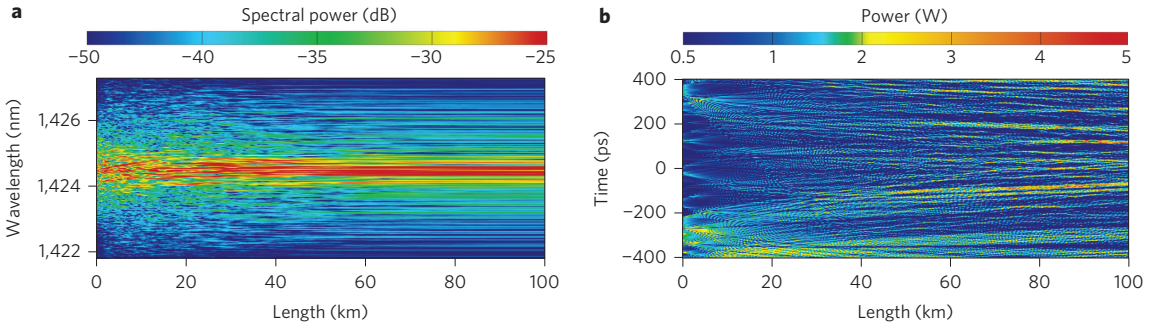

Figure 3 | Evolution of the signal spectrum and temporal shape along the fibre. a, Computed power spectrum density evolution along the LEAF fibre, demonstrating a transition to very stable propagation with a distinctive asymptotic spectrum. **b**, Corresponding spatiotemporal dynamics over an interval of 800 ps. Here, the fluctuating c.w. power $P(t,z)$ is normalized by the distance-dependent factor $P_{norm}(z) = P(0)\exp(\alpha z)$, where $\alpha = 0.25$ dB km^{-1} is the fibre loss. The two figures illustrate that although the temporal field structure is irregular, the spectrum propagation demonstrates remarkable stability.

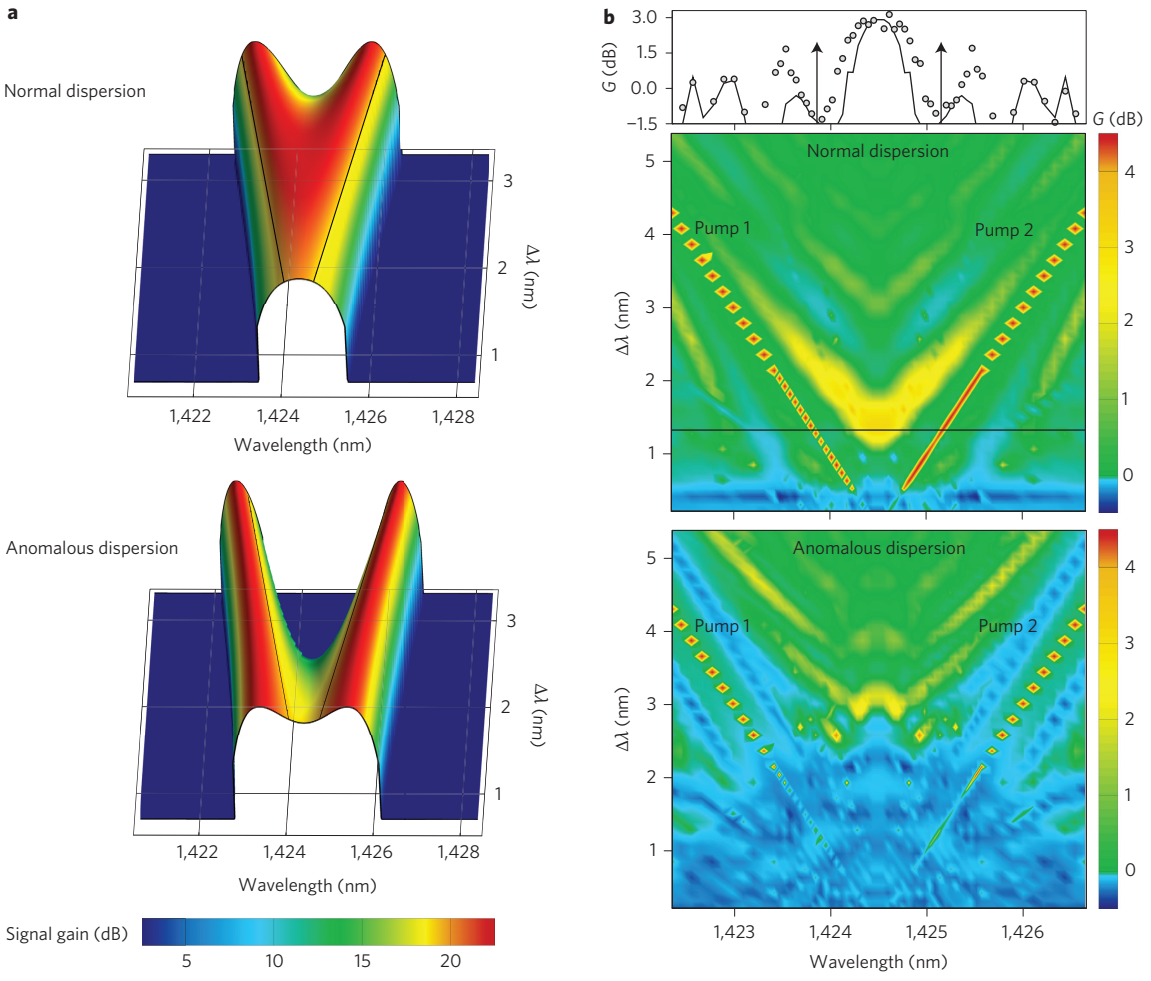

Figure 4 | Signal gain spectra as a function of pump wavelength spacing. a, Four-wave model, $P_0(0) = 1.5$ W, $L = 1$ km. The unsaturated single-pass gain for signal G_3 is shown. Black lines show the corresponding wavelengths of the pumps. **b**, NLSE model, $P_0(0) = 1.5$ W, $P_3(0) = 300$ mW, $P_4(0) = 0$, $L = 1$ km. The projection at the top is related to the normal dispersion case: black solid line, deterministic phases of waves; grey circles, averaging over 600 sets of random phases.

dynamics of the signal features highly irregular intensity fluctuations (Fig. 3b). Despite visible irregularities in the temporal field distribution shown in Fig. 3b, in the spectral domain this statistical steady state is very stable and may evolve without major changes over long distances. Due to the fact that multiple modes are involved in building this statistical equilibrium through nonlinear FWM interactions, the process calls for a kinetic description[13,27]. We believe that this is an interesting and practically important experimental observation of kinetic equilibrium in optical fibre[8,10,12,13,27].

We performed a number of experiments with various fibres at different wavelengths, as well as extensive numerical modelling, and conclude that we were able to observe the effect of nonlinear spectral narrowing only in the case of normal fibre dispersion (Supplementary Note 1).

Qualitative analysis

First let us try to explain qualitatively the physical mechanism underlying the spectral narrowing of a high-power field containing many longitudinal modes in normal dispersion fibre. The key idea came from the observation that the Raman laser output (with its double-peaked spectrum) being launched into the LEAF fibre resembles a two-pump OPA with two spectrally separated pumps. Of course, there are no separate 'pumps' and 'signal' in this case. Instead, the input field self-acts by redistributing energy from the peripheral wavelengths (pumps) to the central region (signal). This is obviously only a qualitative picture that helps in understanding the main elementary mechanism of such self-pumping of the central wavelength region at the expense of the tails. Consider those effective pumps to be at frequencies ω_1 and ω_2 at the fibre input. Such effective pumps would amplify the signal and idler with frequencies ω_3 and ω_4, respectively. Consider, $\omega_1 < \omega_2$ and $\omega_3 < \omega_4$. Here, evidently, the signal and idler represent just two spectral components of the same wave packet that, through FWM, obtain energy from the tails of the spectrum (pumps). Note that ω_3 and ω_4 are symmetric with respect to the centre frequency $\omega_c = (\omega_1 + \omega_2)/2 = (\omega_3 + \omega_4)/2$, which is halfway between the two pump frequencies. In fact, the SPA effect does not require a two-pump structure of the input field; similar spectral narrowing can be observed for input waves with a bell-shaped spectrum. This was conclusively confirmed by additional experiments and modelling (see Supplementary Section 'Gain analysis in the NLSE model' and the Supplementary materials). The particular example considered here is very useful for understanding the underlying principle; that is, the two spectral peaks in the Raman laser output could be associated with the pumps, whereas the spectral narrowing of the laser output as it propagates in the normal dispersion fibre could be associated with the signal and idler (or just the signal if $\omega_3 = \omega_4$) amplification in an effective fibre OPA.

In this qualitative analysis, consider first the undepleted pump case when signal and idler are small compared to the pumps $P_3 \ll P_0 = P_1 + P_2$ (for simplicity, as the analysis in this section is only qualitative, formulae here are given for the case when the idler is absent at $z = 0$). The unsaturated single-pass gain for the signal, G_3, may be written as[15,17]

$$G_3 = \frac{P_3(L)}{P_3(0)} = 1 + \left[\frac{\gamma P_0}{g}\sinh(gL)\right]^2 \quad (1)$$

where the idler gain is $G_4 = G_3 - 1$, g is a parametric gain coefficient given by $g^2 = r^2 - (k/2)^2$, $r = \gamma P_0$, and γ is a nonlinearity coefficient. The gain coefficient reaches its maximum value when $k = \Delta\beta + \Delta\beta_{NL} = 0$, where k is the total propagation constant, $\Delta\beta = \beta(\omega_3) + \beta(\omega_4) - \beta(\omega_1) - \beta(\omega_2)$ is the propagation constant mismatch and $\Delta\beta_{NL} = \gamma P_0$ is the nonlinear contribution to the wavevector mismatch. The corresponding single pass signal gain is equal to

$$G_{3,\max} = 1 + (\sinh(\gamma P_0 L))^2 \quad (2)$$

and for the idler

$$G_{4,\max} = (\sinh(\gamma P_0 L))^2$$

It is convenient to introduce the following notation: $\Delta\omega_s = \omega_3 - \omega_c$, $\Delta\omega_p = \omega_1 - \omega_c = \omega_c - \omega_2$. To understand the effect of dispersion, we can expand the propagation constant mismatch in a standard power series in terms of $\Delta\omega_s$ and $\Delta\omega_p$ (refs 15,17): $\Delta\beta = 2\sum_{m=1}^{\infty}(\beta_{2m}/(2m)!)[(\Delta\omega_s)^{2m} - (\Delta\omega_p)^{2m}]$, where β_{2m} are even derivatives of $\beta(\omega)$ at ω_c. Consider only the main term in this expansion assuming that $\beta_4 \ll \beta_2$; that is, $\Delta\beta \approx \beta_2[(\Delta\omega_s)^2 - (\Delta\omega_p)^2]$. The shape of the gain spectrum and location of the gain maximum in the spectral domain are given by the condition of phase matching:

$$k = 0 \Rightarrow \left[(\Delta\omega_s)^2 - (\Delta\omega_p)^2\right] = \frac{-\gamma P_0}{\beta_2} \quad (3)$$

Equation (3) provides a reasonable qualitative explanation of why the sign of the dispersion matters in the considered experiment. When the fibre dispersion is normal ($\beta_2 > 0$), the gain maximum is located between the pumps and $\Delta\omega_s < \Delta\omega_p$, but when the fibre dispersion is anomalous ($\beta_2 < 0$), the gain maximum is located outside the area between the pumps, in the frequency domain $\Delta\omega_s > \Delta\omega_p$ (Fig. 4a). Figure 4a depicts the signal parametric gain G_3 (in dB) as a function of distance $\Delta\lambda$ between the pumps and signal wavelength. Black lines show the wavelengths of the pumps. In the normal dispersion regime the gain spectrum is bell-shaped, with the maximum amplification in its central part. When the dispersion is anomalous, symmetric gain maxima are always located outside the area between the pumps, which effectively leads to significant spectrum broadening.

Note that, for a central frequency gain, when the signal coincides with the idler ($\Delta\omega_s = 0$), we have degenerate OPA and signal amplification should be considered in the framework of the degenerate OPA model. The qualitative analysis presented in this section explains the difference between normal and anomalous dispersion propagation regimes. However, this simple model does not take into account pump depletion and the generation of additional waves through FWM. This changes the quantitative characteristics

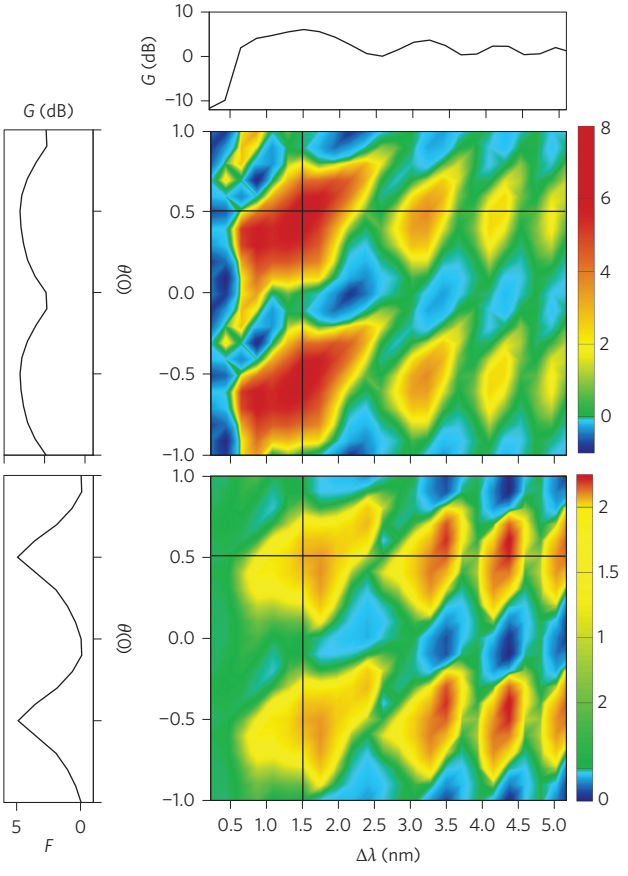

Figure 5 | Estimate of FWM product during signal amplification. Top: dependence of signal gain G (in dB) on relative phase difference $\theta(0)$ and wavelength spacing between two pumps $\Delta\lambda$. Bottom: dependence of $F = \Delta P_s/P_{FWM}$ on relative phase difference $\theta(0)$ and wavelength spacing between two pumps $\Delta\lambda$.

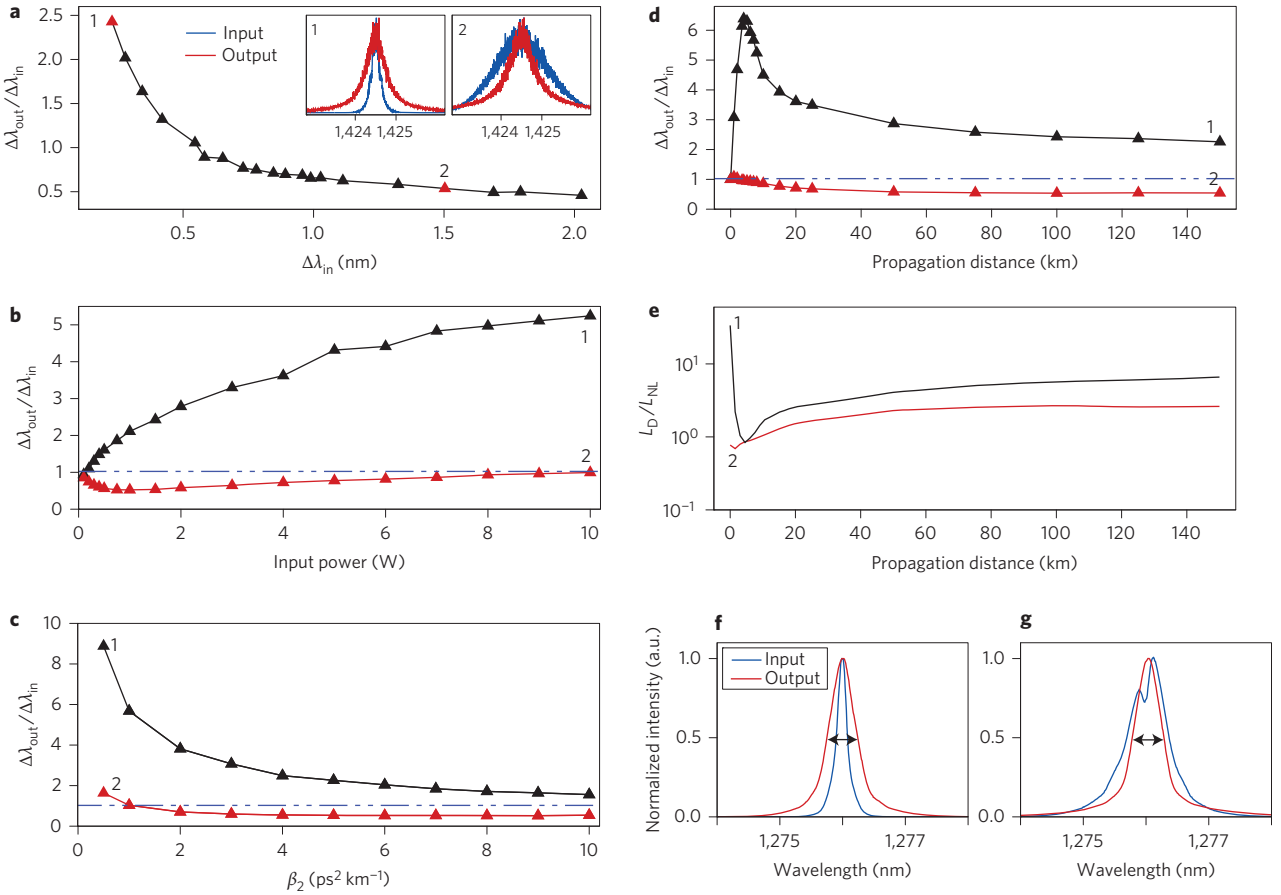

Figure 6 | Theoretical evolution of the spectral broadening factor. a, Dependence of the broadening factor $\Delta\lambda_{out}/\Delta\lambda_{in}$ on the initial spectrum width $\Delta\lambda_{in}$ after 100 km of LEAF, $P_0 = 1.5$ W, lossless fibre. Inset: spectrum shapes before and after signal propagation in 100 km of LEAF, corresponding to the points marked 1 and 2. **b**, Dependence of the broadening factor $\Delta\lambda_{out}/\Delta\lambda_{in}$ on pump power, corresponding to the points marked 1 and 2, $L = 100$ km. **c**, Dependence of the broadening factor $\Delta\lambda_{out}/\Delta\lambda_{in}$ on group delay dispersion, corresponding to the points marked 1 and 2, $L = 100$ km, $P_0 = 1.5$ W. **d**, Dependence of the broadening factor $\Delta\lambda_{out}/\Delta\lambda_{in}$ on fibre length, corresponding to the points marked 1 and 2, $P_0 = 1.5$ W. **e**, Scaling of L_d/L_{NL} along the propagation distance ($P_0 = 1.5$ W). **f**,**g**, Experimentally measured input and output spectra of 1,276 nm light propagating in 100 km of SMF-28 versus input power with $P_0 = 0.7$ W (**f**) and $P_0 = 1.3$ W (**g**).

of the SPA process and requires a more accurate analysis (presented in the following section).

Gain analysis in the NLSE model

The four-wave model described above gives only a qualitative picture. Many other frequency components are generated and interact with each other due to FWM in the process under consideration. Some of these waves may be well phase-matched and so may reach levels comparable with the signal. To give a more realistic evaluation of the SPA we now use the NLSE to obtain the signal amplification spectrum in the presence of parasitic FWM components depleting the effective gain. Figure 4b shows the signal gain spectrum corresponding to the two-pump fibre OPA with varying distance between the pumps. Here, the total pump power is 1.5 W, the signal c.w. power at the fibre input is 300 mW and the idler is absent at $z = 0$. The gain spectrum is still bell-shaped if the distance between the pumps is properly chosen (Fig. 4b, top, solid lines), and maximum amplification is achieved in the frequency band between the pumps.

Note that we previously considered an ideal case—a phase-insensitive parametric amplifier. The real laser output has the form of a multimode light field without phase locking, so the SPA of such a field is phase-sensitive. To study the impact of the effect of random initial phases we performed additional simulations. We considered a signal and idler with equal powers (300 mW total power) at the fibre input, and the relative phase difference between the four involved light waves at the fibre input $\theta(0) = \varphi_1(0) + \varphi_2(0) - \varphi_3(0) - \varphi_4(0)$ was assumed to be a random value with a uniform probability distribution bounded between $-\pi$ and π. Statistical analysis was performed with 600 different sets of random phases. A statistical signal gain spectrum averaged over the 600 sets is shown by grey circles in Fig. 4b, top. It has a characteristic high peak at the central frequency, similar to the simplified four-wave model.

Although we have shown that the maximum signal amplification can be achieved near the central frequency, new spectral components could still be amplified simultaneously with the signal and lead to broadening of the laser spectrum. To investigate pump energy transfer along the fibre, we consider signal amplification at the central frequency (where the signal coincides with the idler, $\omega_c = \omega_3 = \omega_4$). To estimate the value of the FWM product during signal amplification we introduce the dimensionless function $F(\Delta\lambda,\theta(0))$, defined as the ratio between the pump energy transferred to the signal at frequency $\omega = \omega_3$ and the pump energy transferred to other frequencies due to FWM: $F = \Delta P_s/P_{FWM}$, where $\Delta P_s = P_3(L) - P_3(0)$ and $P_{FWM} = P_0(0) + P_3(0) - P_p(L) - P_3(L)$. $F(\Delta\lambda,\theta(0))$ is a figure of merit indicating how effectively pump energy transfers to the signal, that is, the efficiency of signal

amplification. $F = 0$ corresponds to $G_3 = 0$ (that is, no amplification for the ω_3 signal), whereas F tends to infinity when the only spectral component amplified is the ω_3 signal.

Figure 5 shows the value of the signal gain $G = 10\log_{10}(P_s(L)/P_s(0))$ and dimensionless function F (bottom row) in the plane of parameters $\Delta\lambda - \theta(0)$. It can be seen that the FWM product can be neglected if the spectral distance between the pumps is properly chosen (undesirable FWM product is minimized and all the pump energy transfers to the signal).

Discussion

An interesting question is 'What are the conditions for spectral compression and broadening in normal dispersion fibre?' In Fig. 6 we considered the broadening factor $\Delta\lambda_{out}/\Delta\lambda_{in}$ as a function of initial spectral width, power, fibre dispersion and cavity length. Figure 6a depicts the evolution of the broadening factor $\Delta\lambda_{out}/\Delta\lambda_{in}$ with an initial spectrum width $\Delta\lambda_{in}$ in numerical simulations. When the spectrum width at $z = 0$ is less than 0.5 nm, we still observe spectrum broadening in a 100-km-long fibre. However, if $\Delta\lambda_{in}$ exceeds 0.5 nm, spectrum narrowing takes place. We verified that this effect is observed both in lossy and lossless cases (for details see Supplementary Note 2). We also studied the impact of dispersion (Supplementary Note 3) and the statistics of the compressing signal (Supplementary Note 4). In Fig. 6b–e we consider in more detail two different points along the line, corresponding to spectrum broadening and narrowing (marked 1 and 2 in Fig. 6a). For $\Delta\lambda_{in} = 0.23$ nm, the broadening factor first monotonically increases with fibre length L as long as it is shorter than 5 km (Fig. 6d). With a further increase of the propagation distance, the initial rise is followed by a decrease. This kind of evolution of a multimode c.w. field was previously observed in ref. 32. Scaling of L_d/L_{NL} along the propagation distance is shown in Fig. 6e. Spectral broadening occurs when the dispersion length at the fibre input is much greater than the nonlinear length. On the other hand, when the dispersion length becomes comparable with the nonlinear length, we observe nonlinear spectral narrowing. The observed nonlinear spectral broadening depends on the ratio of the dispersive and nonlinear lengths L_d/L_{NL}. Light with a broader bandwidth can therefore also be compressed provided that after rescaling of the parameters the factor L_d/L_{NL} is the same as in the studied examples.

We also experimentally verified that the RFL spectrum narrows when transmitted through other fibres with normal dispersion (Fig. 6f,g). Laser radiation generated at 1,276 nm was launched into the same 100 km length of SMF-28, which has normal dispersion at this wavelength ($\beta_2 = 3.1$ ps^2 km^{-1}, $\gamma = 1.8$ W^{-1} km^{-1}). We observed spectral narrowing both in the experiment and simulation. In the experiment, a narrow and low-power (0.7 W) RFL spectrum becomes broader after propagation in SMF (Fig. 6f). However, when the initial width and power increase (1.3 W), one can observe compression (Fig. 6g) and the formation of a stable spectrum.

The remarkable spectral stability of the evolved state (in normal dispersion fibre), despite a random temporal behaviour, indicates that we observe an asymptotic kinetic regime resulting from the optical wave turbulence of a multitude of elementary waves in the nonlinear system considered[8,10,12,13,34]. It is also worth pointing out that this surprising finding that the evolved spectral distribution does not change appreciably with propagation may potentially be exploited in fibre lasers and optical telecommunications. In fibre lasers, nonlinear compression may lead to increased spectral brightness compared to systems using direct spectral filtering, thereby avoiding the additional losses inevitable with filters. In optical communications, spectrally stable nonlinear propagation regimes may lead to new techniques for mitigation of the nonlinear transmission impairments that are a major challenge in modern high-capacity systems.

Conclusion

We have presented a new self-action effect—self-parametric amplification or inverse FWM, that may occur during high-power wave propagation in normal dispersion fibre and that manifests itself as a spectral compression of light. This is different from the compression of pre-chirped coherent pulses[35–40]. The observed effect is the result of a nonlinear energy redistribution from the tails of the signal spectrum to the central region. This can be considered as an effective SPA of the central part of the wave packet spectrum by the peripheral pumps. The presented simple theory of SPA explains all the key features observed in the experiments and full numerical modelling. We believe that the remarkable stability of the observed spectral field distribution may offer new interesting applications in high-power fibre lasers and optical telecommunications.

Methods

Methods and any associated references are available in the online version of the paper.

Received 6 March 2015; accepted 13 July 2015;
published online 10 August 2015

References

1. Stolen, R. H. The early years of fiber nonlinear optics. *J. Lightw. Technol.* **26,** 1021–1031 (2008).
2. Agrawal, G. P. *Nonlinear Fiber Optics* (Academic, 2007).
3. Boyd, R. W. *Nonlinear Optics* (Academic, 2003).
4. Toulouse, J. Optical nonlinearities in fibers: review, recent examples, systems applications. *J. Lightw. Technol.* **23,** 3625–3641 (2005).
5. Dudley, J. M. & Taylor, J. R. Ten years of nonlinear optics in photonic crystal fibre. *Nature Photon.* **3,** 85–90 (2009).
6. Garmire, E. Nonlinear optics in daily life. *Opt. Express* **21,** 30532–30544 (2013).
7. Solli, D. R., Ropers, C., Koonath, P. & Jalali, B. Optical rogue waves. *Nature* **450,** 1054–1057 (2007).
8. Turitsyna, E. G. *et al.* The laminar–turbulent transition in a fibre laser. *Nature Photon.* **7,** 783–786 (2013).
9. Kibler, B. *et al.* The Peregrine soliton in nonlinear fibre optics. *Nature Phys.* **6,** 790–795 (2010).
10. Turitsyn, S. K. *et al.* Random distributed feedback fibre laser. *Nature Photon.* **4,** 231–235 (2010).
11. Turitsyn, S. K., Bale, B. & Fedoruk, M. P. Dispersion-managed solitons in fibre systems and lasers. *Phys. Rep.* **521,** 135–203 (2012).
12. Turitsyn, S. K. *et al.* Random distributed feedback fibre lasers. *Phys. Rep.* **542,** 133–193 (2014).
13. Picozzi, A. *et al.* Optical wave turbulence: toward a unified nonequilibrium thermodynamic formulation of statistical nonlinear optics. *Phys. Rep.* **542,** 1–132 (2014).
14. Stolen, R. H. Phase-matched-stimulated four-photon mixing in silica-fiber waveguides. *IEEE J. Quantum Electron.* **11,** 100–103 (1975).
15. Marhic, M. E. *Fiber Optical Parametric Amplifiers, Oscillators and Related Devices* (Cambridge Univ. Press, 2007).
16. Hansryd, J., Andrekson, P. A., Westlund, M., Li, J. & Hedekvist, P. O. Fiber-based optical parametric amplifiers and their applications. *J. Sel. Top. Quantum Electron.* **8,** 506–520 (2002).
17. Radic, S. & McKinstrie, C. J. Two-pump fiber parametric amplifiers. *Opt. Fiber Technol.* **9,** 7–23 (2003).
18. McKinstrie, C. & Radic, S. Phase-sensitive amplification in a fiber. *Opt. Express* **12,** 4973–4979 (2004).
19. McKinstrie, C. J., Radic, S. & Gnauck, A. H. All-optical signal processing by fiber-based parametric devices. *Opt. Photon. News* **18,** 34–40 (2007).
20. Marhic, M. E. *et al.* Fiber optical parametric amplifiers in optical communication systems. *Laser Photon. Rev.* **9,** 50–74 (2015).
21. Tong, Z. *et al.* Towards ultrasensitive optical links enabled by low-noise phase-sensitive amplifiers. *Nature Photon.* **5,** 430–436 (2011).
22. Slavik, R. *et al.* All-optical phase and amplitude regenerator for next-generation telecommunications systems. *Nature Photon.* **4,** 690–695 (2010).
23. Karpov, V. I., Clements, W. R. L., Dianov, E. M. & Papernyi, S. B. High-power 1.48 μm phosphoro-silicate-fiber-based laser pumped by laser diodes. *Can. J. Phys.* **78,** 407–413 (2000).
24. Bouteiller, J-C. Spectral modeling of Raman fiber lasers. *Photon. Technol. Lett.* **15,** 1698–1700 (2003).
25. Suret, P. & Randoux, S. Influence of spectral broadening on steady characteristics of Raman fiber lasers: from experiments to questions about the validity of usual models. *Opt. Commun.* **237,** 201–212 (2004).

26. Turitsyn, S. K. *et al.* Modeling of CW Yb-doped fiber lasers with highly nonlinear cavity dynamics. *Opt. Express* **19,** 8394–8405 (2011).
27. Babin, S., Churkin, D., Ismagulov, A., Kablukov, S. & Podivilov, E. Four-wave-mixing-induced turbulent spectral broadening in a long Raman fiber laser. *J. Opt. Soc. Am. B* **24,** 1729–1738 (2007).
28. Turitsyn, S. K. *et al.* in *Advances in Wave Turbulence* Vol. 83 (eds Shrira, V. & Nazarenko, S.) Ch. 4, 113–164 (World Scientific Series on Nonlinear Science Series A, World Scientific, 2013).
29. Babin, S. *et al.* Turbulent broadening of optical spectra in ultralong Raman fiber lasers. *Phys. Rev. A* **77,** 033803 (2008).
30. Paramonov, V. M., Kurkov, A. S., Medvedkov, O. I., Grukh, D. A. & Dianov, E. M. Two-frequency fibre Raman laser. *Quantum Electron.* **34,** 213–215 (2004).
31. Turitsyna, E. G., Falkovich, G., Mezentsev, V. K. & Turitsyn, S. K. Optical turbulence and spectral condensate in long-fiber lasers. *Phys. Rev. A* **80,** 031804 (2009).
32. Barviau, B., Randoux, S. & Suret, P. Spectral broadening of a multimode continuous-wave optical field propagating in the normal dispersion regime of a fiber. *Opt. Lett.* **31,** 1696–1698 (2006).
33. Churkin, D., Smirnov, S. & Podivilov, E. Statistical properties of partially coherent cw fiber lasers. *Opt. Lett.* **35,** 3288–3290 (2010).
34. Churkin, D. V. *et al.* Wave kinetics of random fibre lasers. *Nature Commun.* **6,** 6214 (2015).
35. Sidorov-Biryukov, D. A. *et al.* Spectral narrowing of chirp-free light pulses in anomalously dispersive, highly nonlinear photonic-crystal fibers. *Opt. Express* **16,** 2502–2507 (2008).
36. Cundiff, S. T. *et al.* Propagation of highly chirped pulses in fiber-optic communications systems. *J. Lightw. Technol.* **17,** 811–816 (1999).
37. Washburn, B. R., Buck, J. A. & Ralph, S. E. Transform-limited spectral compression due to self-phase modulation in fibers. *Opt. Lett.* **25,** 445–447 (2000).
38. Planas, S. A., Pires Mansur, N. L., Brito Cruz, C. H. & Fragnito, H. L. Spectral narrowing in the propagation of chirped pulses in single-mode fibers. *Opt. Lett.* **18,** 699–701 (1993).
39. Oberthaler, M. & Höpfel, R. A. Spectral narrowing of ultrashort laser pulses by self-phase modulation in optical fibers. *Appl. Phys. Lett.* **63,** 1017–1019 (1993).
40. Nishizawa, N., Takahashi, K., Ozeki, Y. & Itoh, K. Wideband spectral compression of wavelength-tunable ultrashort soliton pulse using comb-profile fiber. *Opt. Express* **18,** 11700–11706 (2010).

Acknowledgements

The authors acknowledge financial support from the European Research Council project ULTRALASER (267763), the Ministry of Education and Science of the Russian Federation (14.B25.31.0003 and 14.578.21.0029) and the Russian Science Foundation (14-21-00110; work of A.E.B). The authors also thank E. V. Podivilov for fruitful discussions.

Author contributions

S.B.P. initiated the study and carried out the experiments. A.E.B. designed and conducted the numerical modelling. S.K.T., A.E.B. and M.P.F. guided the theoretical and numerical studies. S.K.T., S.B.P., A.E.B., W.R.L.C and M.P.F. analysed the data. S.K.T., A.E.B., S.B.P. and W.R.L.C. wrote the paper.

Additional information

Supplementary information is available in the online version of the paper. Reprints and permissions information is available online at www.nature.com/reprints. Correspondence and requests for materials should be addressed to S.K.T.

Competing financial interests

The authors declare no competing financial interests.

Methods

Propagation in LEAF. Signal propagation down the LEAF fibre was modelled using the NLSE with losses[2]:

$$\frac{\partial A}{\partial z} = -i\frac{\beta_2}{2}\frac{\partial^2 A}{\partial t^2} + i\gamma|A|^2A - \frac{\alpha}{2}A$$

where $A(z,t)$ is the electric field envelope, β_2 is the second-order dispersion coefficient at the central frequency ω_0, $\gamma = n_2\omega_0/(cA_{\mathrm{eff}})$ is the Kerr nonlinearity coefficient with nonlinear refractive index n_2 and effective fibre cross-section area A_{eff} for the fundamental mode, and α is the fibre attenuation coefficient. The equation was solved using the split-step Fourier transform method. The following fibre parameters are used in the simulations: $\beta_2 = 4.3\ \mathrm{ps^2\ km^{-1}}$, $\gamma = 2.16\ \mathrm{W^{-1}\ km^{-1}}$, $\alpha = 0.25\ \mathrm{dB\ km^{-1}}$.

Raman fibre laser. To model the laser generation we used a NLSE-based model previously reported to be efficient for modelling RFLs[33]:

$$\begin{aligned}\frac{\partial A_{\mathrm{p}}^{\pm}}{\partial z} &= -\frac{i}{2}\beta_{2p}\frac{\partial^2 A_{\mathrm{p}}^{\pm}}{\partial t^2} + i\gamma_{\mathrm{p}}[|A_{\mathrm{p}}^{\pm}|^2 + (2-f_R)|A_{\mathrm{s}}^{\pm}|^2]A_{\mathrm{p}}^{\pm}\\ &\quad -\frac{g_{\mathrm{p}}}{2}(|A_{\mathrm{s}}^{+}|^2 + |A_{\mathrm{s}}^{-}|^2)A_{\mathrm{p}}^{\pm} - \frac{\alpha_{\mathrm{p}}}{2}A_{\mathrm{p}}^{\pm} - \frac{\partial A_{\mathrm{s}}^{\pm}}{\partial z} = \left(\frac{1}{v_{\mathrm{s}}} - \frac{1}{v_{\mathrm{p}}}\right)\frac{\partial A_{\mathrm{s}}^{\pm}}{\partial t}\\ &\quad -\frac{i}{2}\beta_{2\mathrm{s}}\frac{\partial^2 A_{\mathrm{p}}^{\pm}}{\partial t^2} + i\gamma_{\mathrm{s}}[|A_{\mathrm{s}}^{\pm}|^2 + (2-f_R)|A_{\mathrm{p}}^{\pm}|^2]A_{\mathrm{p}}^{\pm}\\ &\quad +\frac{g_{\mathrm{s}}}{2}(|A_{\mathrm{p}}^{+}|^2 + |A_{\mathrm{p}}^{-}|^2)A_{\mathrm{s}}^{\pm} - \frac{\alpha_{\mathrm{s}}}{2}A_{\mathrm{s}}^{\pm}\end{aligned} \tag{4}$$

The boundary conditions describe the pump input and the reflection of the optical field from the fibre Bragg gratings:

$$A_{\mathrm{p}}^{+}(0,t) = A_{\mathrm{in}},\ A_{\mathrm{p}}^{-}(L,\omega) = \sqrt{R_{\mathrm{p}}(\omega)}A_{\mathrm{p}}^{+}(L,\omega)$$

$$A_{\mathrm{s}}^{+}(0,\omega) = \sqrt{R_{\mathrm{in}}(\omega)}A_{\mathrm{s}}^{-}(0,\omega),\ A_{\mathrm{s}}^{-}(L,\omega) = \sqrt{R_{\mathrm{out}}(\omega)}A_{\mathrm{s}}^{+}(L,\omega)$$

where $R_{\mathrm{in}}(\omega)$ and $R_{\mathrm{out,p}}(\omega)$ are the reflectivities (with respect to power) at the left and right cavity ends, respectively.

The model describes spectral broadening during one roundtrip and the building of a steady state over many roundtrips. We integrated equations (4) along z using the split-step Fourier transform method and an iterative procedure similar to that used for the modelling of Brillouin fibre lasers[41]. For example, to integrate the equation for $A_{\mathrm{s,p}}^{\pm}(z,t)$ we substituted into the equation $A_{\mathrm{s,p}}^{\mp}(z,t)$obtained from a previous iteration, and so on. The generation becomes stable after 10^2–10^4 roundtrips, depending on the power.

References

41. Preda, C. E., Fotiadi, A. A. & Mégret, P. Numerical approximation for Brillouin fiber ring resonator. *Opt. Express* **20,** 5783–5788 (2012).

nature photonics

SUPPLEMENTARY INFORMATION

DOI: 10.1038/NPHOTON.2015.150

Inverse four-wave-mixing and self-parametric amplification in optical fibre

Sergei K. Turitsyn, Anastasia E. Bednyakova, Mikhail P. Fedoruk, Serguei B. Papernyi & Wallace R.L. Clements

Supplementary Note 1. Spectral evolution of optical signal in different types of fibre.

To prove the generality of a new inverse FWM process, we experimentally investigated signal propagation in normal and anomalous dispersion fibres of different types, namely, SMF-28, LEAF, LS and TrueWave RS.

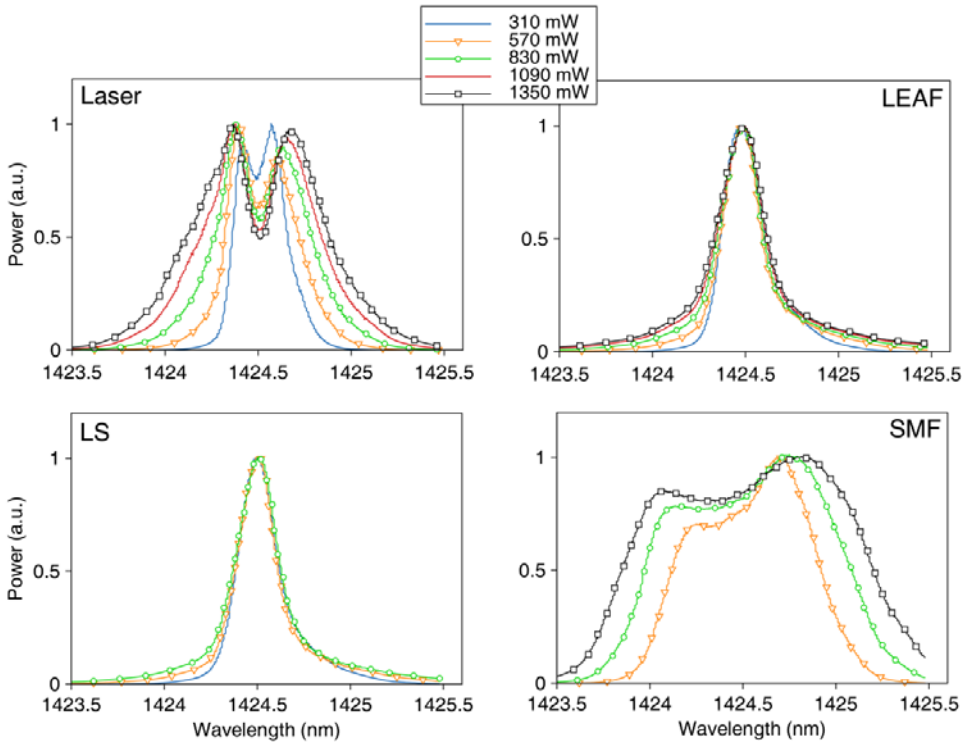

Supplementary Figure 1: Spectrum evolution in fibres of different types. Experimentally measured input and output spectra of 1424-nm light propagating in 100 km of LEAF, LS and

DOI: 10.1038/NPHOTON.2015.150

SMF-28. L_d / L_{NL} scales from 4 to 2.5 at LEAF and LS inputs and from 1.2 to 3 at SMF input with the laser power growth.

First, a signal at 1425 nm was launched into 100 km of SMF-28, LEAF and LS (see Supplementary Fig. 1). As expected, we observed spectral narrowing in the normal dispersion fibre (LS and LEAF) and broadening in SMF. The various lines here correspond to different input powers.

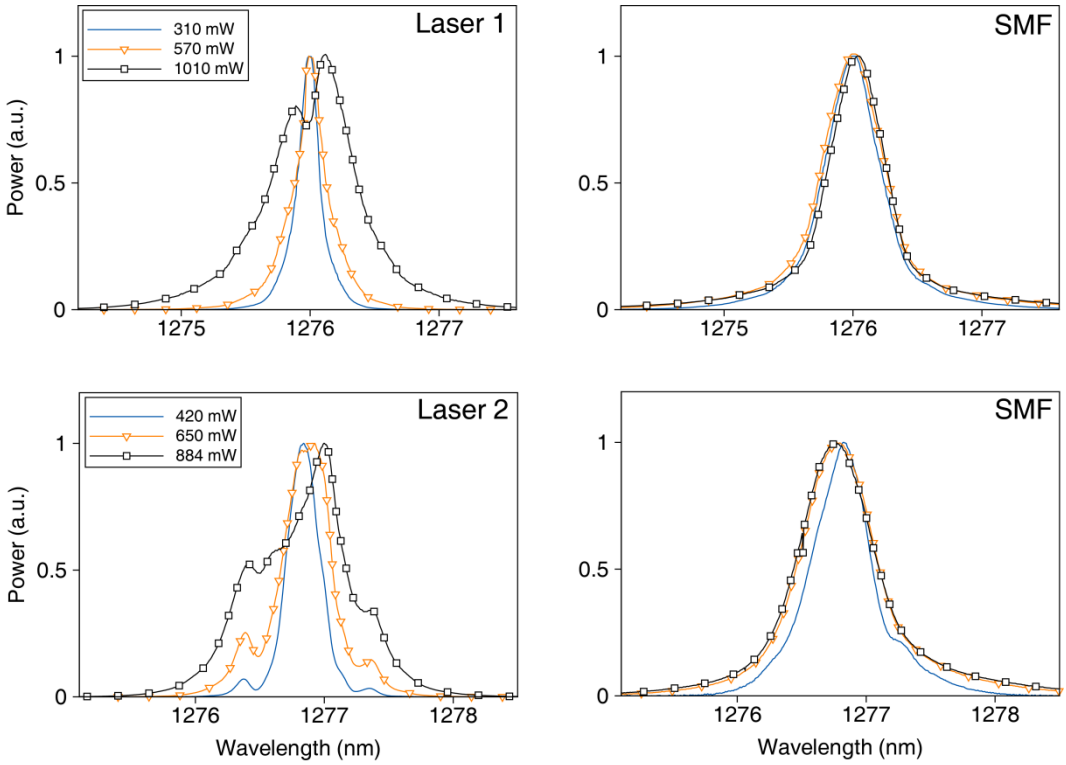

Supplementary Figure 2: Spectrum evolution in SMF. Experimentally measured input and output spectra of signal propagating in 100 km of SMF-28. Two lasers operating at 1276 and 1277 nm were used. L_d / L_{NL} scales from 8 (broadening) to 1.9 (compression) at SMF input with the laser (1276 nm) power growth.

Next we considered signal propagation in SMF in the normal dispersion regime (Supplementary Fig. 2). We used two different lasers and, with both lasers, we observed spectral compression for relatively broad input spectra and broadening for narrow input spectra, as is described in the Discussion section. Double-peaked spectra are usually relatively broad and that is why we always observe its compression in normal dispersion fibres. This example together with Supplementary Fig. 1 shows that broadening or compression can be observed in the same fibre when one operates it in different dispersion regions (anomalous dispersion – broadening, and normal dispersion – compression).

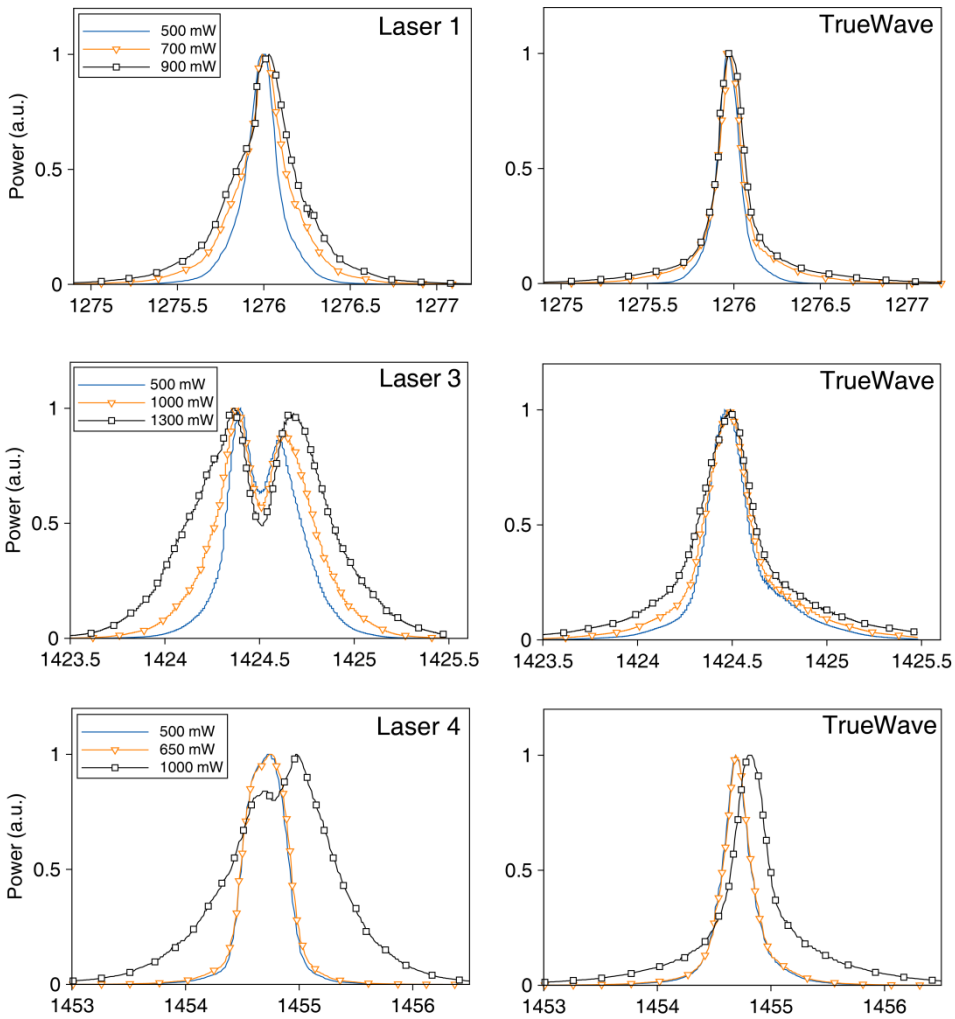

DOI: 10.1038/NPHOTON.2015.150

Supplementary Figure 3: Spectrum evolution in TrueWave. Experimentally measured input and output spectra of signal propagating in 25 km of TrueWave RS. Three laser inputs generated at 1276, 1424 and 1455 nm were considered. L_d / L_{NL} scales from 5 to 2.6 at 1276 nm, from 3.6 to 2.4 at 1424.5 nm and from 5.8 to 2.3 at 1455 nm with the lasers power growth.

We also investigated spectrum propagation in the same fibre, but at different wavelengths (corresponding to different values of dispersion). The results are presented in Supplementary Fig. 3. Signals from three lasers operating at 1424, 1455 and 1276 nm were launched into 25 km of "TrueWave RS" fibre with a zero dispersion wavelength (ZDW) around 1480-1500 nm. The results showing characteristic spectral narrowing for a wide input spectrum are depicted in the figures above. We would like to note that the 1455-nm signal was close to the zero dispersion wavelength and the input signal at 1276 nm was far away from the zero dispersion point.

We have also performed experiments with a hybrid propagation configuration (i.e. combining two types of fibre). Supplementary Fig. 4 (left) shows spectrum after the output of a laser (with a spectrum shown by the blue curve) propagated through 5.5 km of SMF28 fibre. The power exiting the end of the SMF span was 670 mW and the spectrum of the output is shown by the green dashed curve. Next, this 5.5-km piece of SMF28 was spliced to 25 km of TrueWave fibre. The spectrum of output at the end of the combined SMF+TrueWave fibre span is shown by red line. Then, we attenuated the output of the laser down to 670 mW (to make it similar to the power after the SMF in the hybrid fibre span propagation) and launched it into the 25 km of TrueWave fibre. The output spectrum after the 25 km of TrueWave fibre is shown by red in the right figure. These experiments show the impact of the initial spectral width of a signal on the

nonlinear compression.

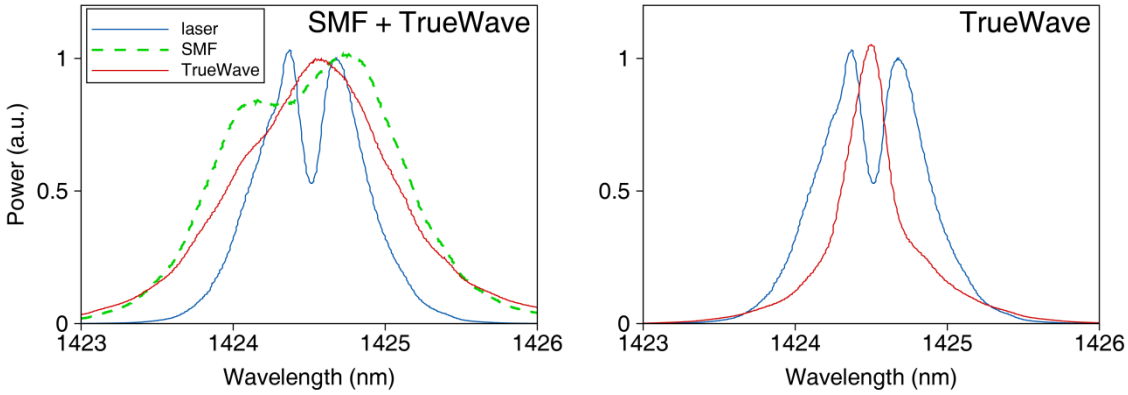

Supplementary Figure 4: Spectrum evolution in the hybrid propagation configuration. Experimentally measured input and output spectra of 1424 nm light propagating in the combined SMF+TrueWave fibre span (left) and TrueWave (right). L_d / L_{NL} equals to 0.5 at SMF input and 1.2 at TrueWave input.

Finally, we additionally checked that similar spectral narrowing can be observed for input waves having a bell-shaped spectrum. A signal with a single-peak spectrum at 1455 nm was launched into 100 km of LEAF. The results are presented in Supplementary Fig. 5.

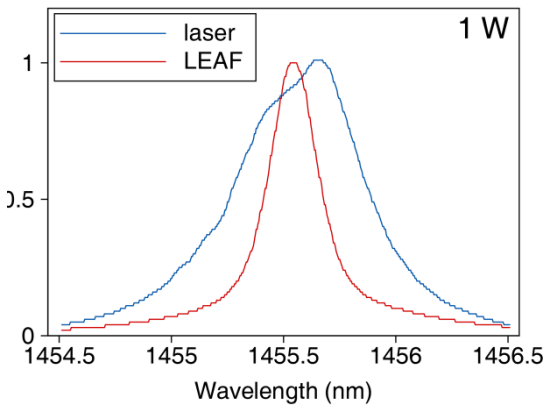

DOI: 10.1038/NPHOTON.2015.150

Supplementary Figure 5: Compression of bell-shaped spectrum in LEAF. Experimentally measured input and output spectra of 1455-nm light propagating in the 100 km of LEAF. $L_d / L_{NL} = 3$ at LEAF input.

Supplementary Note 2. Comparison of signal propagation in lossy and lossless fibres.

Here we demonstrate that the lossless nonlinear Schrödinger equation is a good model for the considered experiments. Supplementary Fig. 6 depicts the numerically computed dependence of the broadening factor $\Delta\lambda_{out} / \Delta\lambda_{in}$ as a function of power, initial spectral width, fibre dispersion and propagation distance. Note that both loss (solid lines) and lossless (dashed lines) cases are shown in this figure. An effective propagation length for L=100 km is about 17.3 km, which can explain the very little difference between the lossy and lossless cases. As could be seen in Supplementary Fig. 6(d), the broadening factor varies slowly after propagation of 20 km distance. Analysis based on the 4-wave model also predicts broadening of the narrow input spectrum (Figure 4(a) of the paper). When the distance between the pumps $\Delta\lambda$ is relatively small, the amplification bandwidth becomes much wider than $\Delta\lambda$, which corresponds to growing energy of the spectrum tails, leading to spectral broadening. On the other hand, when the spectrum width at z = 0 equals 1.5 nm, we discovered monotonic spectrum narrowing with ever decreasing slope along the 100-km long fibre (i.e. the spectral width asymptotically approaches a steady value).

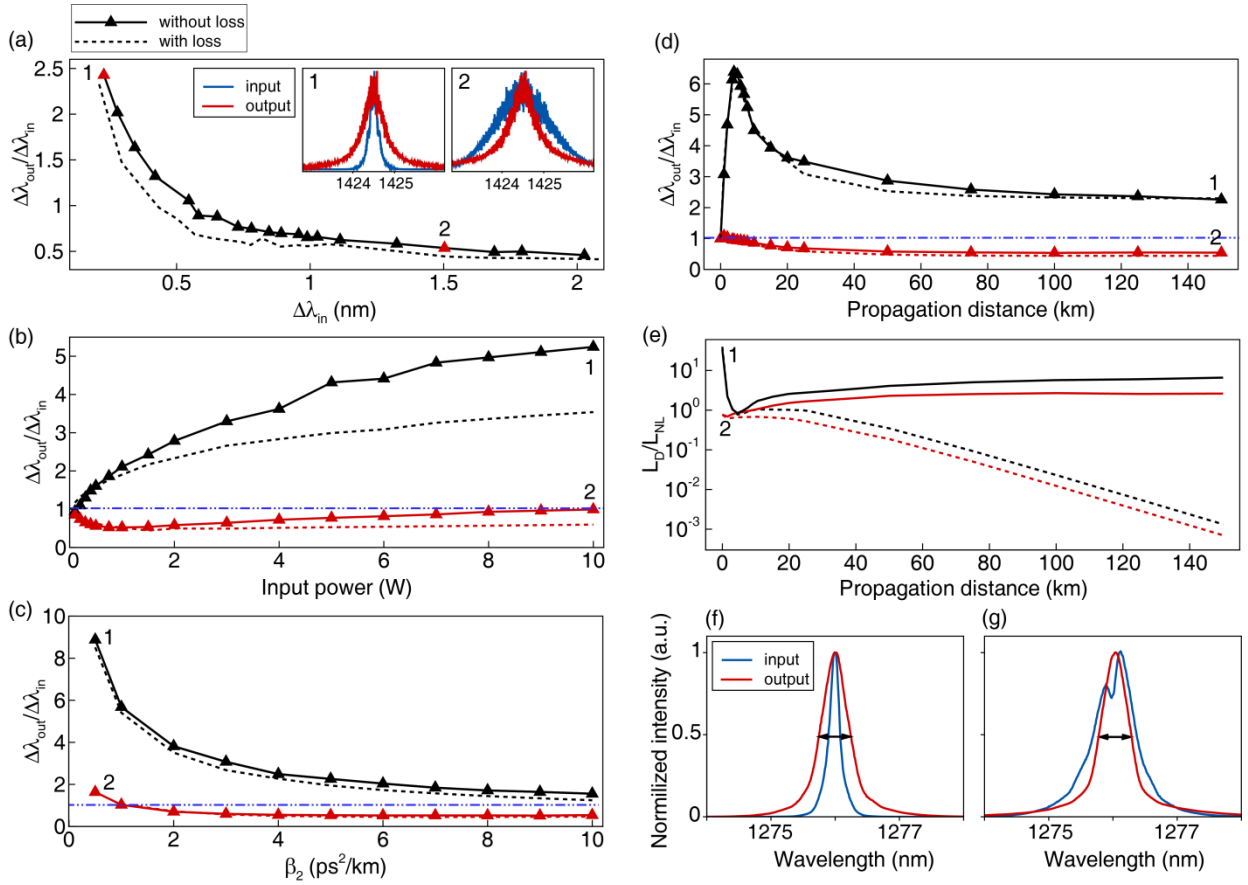

Supplementary Figure 6: Theoretical evolution of the spectral broadening factor. Dependence of the broadening factor $\Delta\lambda_{out} / \Delta\lambda_{in}$ on (**a**) initial spectrum width $\Delta\lambda_{in}$ after 100 km of LEAF, P_0 = 1.5 W. (Inset) Spectrum shapes before and after signal propagation in 100 km of LEAF, corresponding to the points marked "1" and "2"; (**b**) pump power, corresponding to the points marked "1" and "2", L = 100 km; (**c**) group delay dispersion, corresponding to the points marked "1" and "2", L = 100 km, P_0 = 1.5 W; (**d**) fibre length, corresponding to the points marked "1" and "2", P0 = 1.5 W. (**e**) Scaling of L_d / L_{NL} along the propagation distance, P_0 = 1.5 W. (**f,g**) Experimentally measured input and output spectra of 1276-nm light propagating in 100 km of SMF-28 vs. input power (**f**) P_0 = 0.7 W, (**g**) P_0 = 1.3 W. Solid lines denote lossless fiber, dashed lines - fiber with losses.

Supplementary Note 3. Qualitative analysis of the impact of dispersion on spectral compression.

Now, concerning the effect of the third order dispersion (TOD) on the observed spectral compression. The shape of the parametric gain spectrum depends on the propagation constant

DOI: 10.1038/NPHOTON.2015.150

mismatch, signal power and nonlinearity of the fibre (see equations on the page 9 of the paper). At the same time, the propagation constant mismatch $\Delta\beta$ depends only on the even derivatives of $\beta(\omega)$ at ω_c, namely $\beta_2(\omega), \beta_4(\omega)$, etc. and not directly on the odd derivatives $\beta_1(\omega), \beta_3(\omega)$, etc. We varied the signal wavelength in the broad range from 1040 nm to 1550 nm to catch the transition of $\beta_2(\omega)$ from positive to negative values. Supplementary Fig. 7 shows the signal gain spectrum as a function of $\beta_2(\omega)$. Note that we plotted all the spectra at the same central frequency for better visibility. The spectrum dramatically broadens in the vicinity of zero dispersion (this effect is employed in optical parametric amplifiers) and becomes narrower (with maximum in the center) at higher positive dispersion, where spectral compression occurs. This means that spectral compression can't be observed in the vicinity of ZDW. The results of NLSE-based numerical modeling presented in Supplementary Fig. 6(c) also show significant spectral broadening in the vicinity of ZDW.

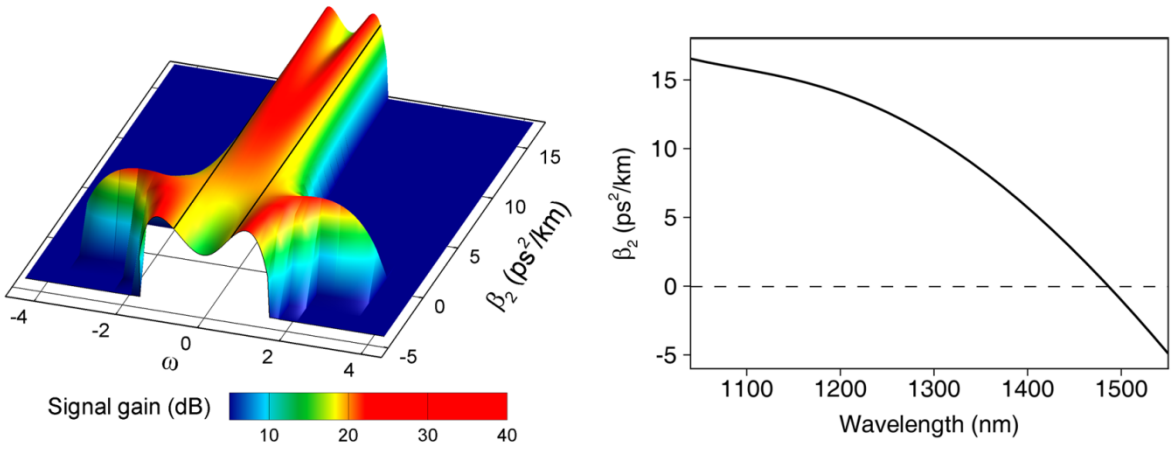

Supplementary Figure 7: Impact of dispersion on spectral compression. Signal gain spectra in LEAF as a function of group delay dispersion $\beta_2(\omega)$ in the 4-wave model. P0 = 1.5 W, L = 1 km, λ_0 =1424 nm.

Supplementary Note 4. Statistical properties of the signal.

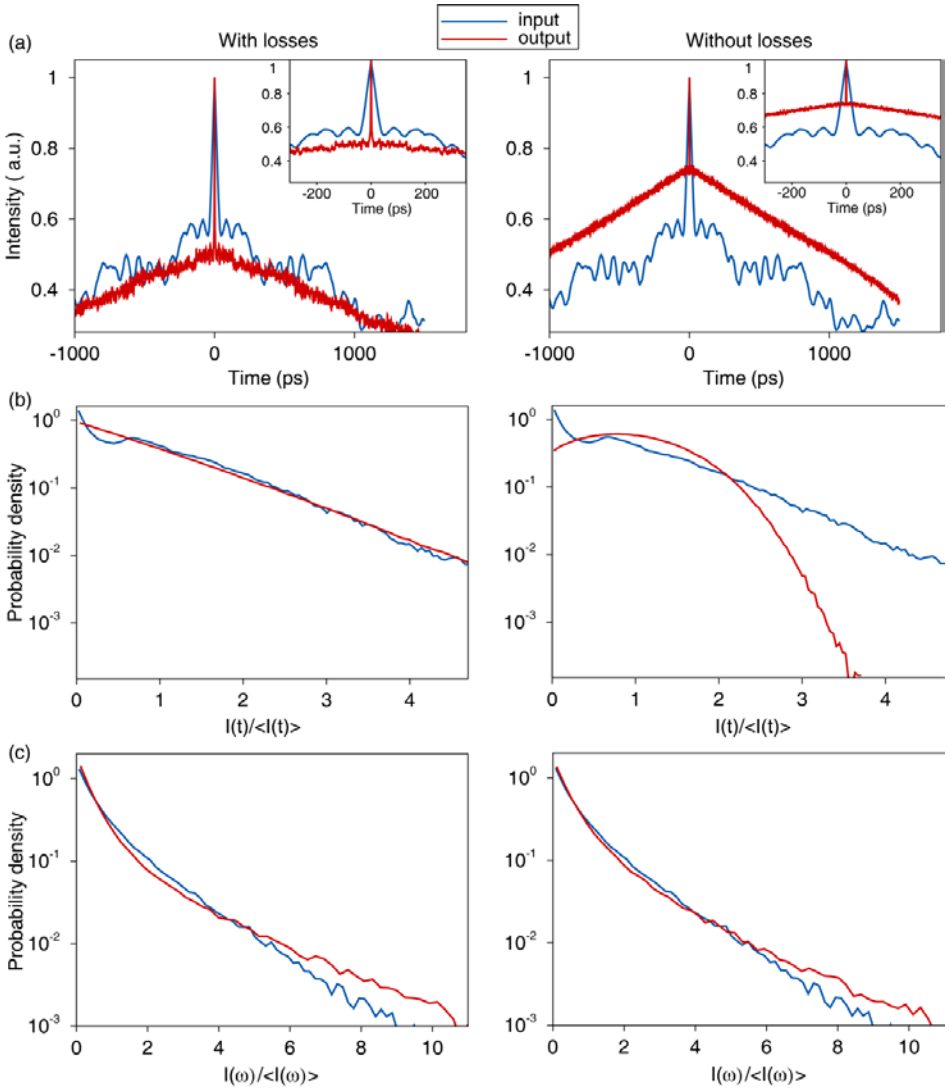

Supplementary Figure 8: Statistical properties of the signal. Intensity autocorrelation (**a**), intensity PDF (**b**) and spectral power density PDF (**c**) in simulation at before and after propagation in 100-km of LEAF. Loss and lossless fibres are considered, P0 = 1.5 W, $\Delta\lambda_{in}$ = 1.5 nm.

Supplementary Fig. 8 shows a statistical analysis of radiation that demonstrates the nontrivial and complex statistical features of the considered effect. In spite of the very similar evolution of

DOI: 10.1038/NPHOTON.2015.150

the broadening factor $\Delta\lambda_{in}$ in the lossy and lossless fibres (see Supplementary Fig. 6), the probability density functions for the intensity fluctuations look quite different in the two cases (Supplementary Fig. 8(b)).

A significant decrease below the Gaussian probability has been observed for intensity fluctuations at the output of LEAF fibre in the lossless case. Supplementary Fig. 8(c) shows the calculated spectral power density PDF for the longitudinal modes of the optical field, lying in the 3-nm spectral band around $\lambda_0 = 1424.5\,\text{nm}$. As could be expected, the graph shows a growing probability of events with higher spectral density and some decrease in probability of events with lower spectral density after propagation in LEAF. The temporal width of the ACF function in numerical modeling decreases from 50 ps at fibre input to 2 ps at fibre output in the both lossy and lossless cases. We attribute the narrowing of the ACF peak to appearance of coherent structures and corresponding short scale correlations in the radiation.